Synthesis of Colloidal Metal Nanocrystals in Droplet Reactors: The Pros and Cons of Interfacial Adsorption

ARTICLE *in* NANO LETTERS · JUNE 2014

Impact Factor: 13.59 · DOI: 10.1021/nl501994q · Source: PubMed

4 AUTHORS, INCLUDING:

Lei Zhang
Zhejiang University
130 PUBLICATIONS **1,097** CITATIONS
SEE PROFILE

Yi Wang
Chongqing Normal University
37 PUBLICATIONS **932** CITATIONS
SEE PROFILE

NANO LETTERS

Letter

pubs.acs.org/NanoLett

Synthesis of Colloidal Metal Nanocrystals in Droplet Reactors: The Pros and Cons of Interfacial Adsorption

Lei Zhang,[†,‡] Yi Wang,[†] Limin Tong,[‡] and Younan Xia*[,†,§]

[†]The Wallace H. Coulter Department of Biomedical Engineering, Georgia Institute of Technology and Emory University, Atlanta, Georgia 30332, United States

[‡]State Key Laboratory of Modern Optical Instrumentation, Department of Optical Engineering, Zhejiang University, Hangzhou 310027, People's Republic of China

[§]School of Chemistry and Biochemistry, School of Chemical and Biomolecular Engineering, Georgia Institute of Technology, Atlanta, Georgia 30332, United States

S *Supporting Information*

ABSTRACT: Droplet reactors have received considerable attention in recent years as an alternative route to the synthesis and potentially high-volume production of colloidal metal nanocrystals. Interfacial adsorption will immediately become an important issue to address when one seeks to translate a nanocrystal synthesis from batch reactors to droplet reactors due to the involvement of higher surface-to-volume ratios for the droplets and the fact that nanocrystals tend to be concentrated at the water−oil interface. Here we report a systematic study to compare the pros and cons of interfacial adsorption of metal nanocrystals during their synthesis in droplet reactors. On the one hand, interfacial adsorption can be used to generate nanocrystals with asymmetric shapes or structures, including one-sixth-truncated Ag octahedra and Au−Ag nanocups. On the other hand, interfacial adsorption has to be mitigated to obtain nanocrystals with uniform sizes and controlled shapes. We confirmed that Triton X-100, a nonionic surfactant, could effectively alleviate interfacial adsorption while imposing no impact on the capping agent typically needed for a shape-controlled synthesis. With the introduction of a proper surfactant, droplet reactors offer an attractive platform for the continuous production of colloidal metal nanocrystals.

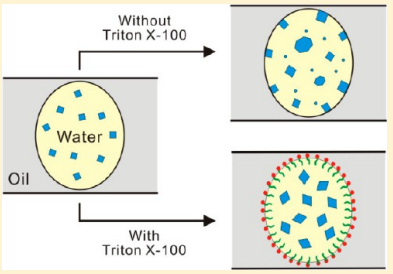

KEYWORDS: *Colloidal nanocrystals, droplet reactors, interfacial adsorption, surfactant*

The past decade has witnessed the successful syntheses of colloidal noble-metal nanocrystals with uniform and controlled compositions, sizes, shapes, and structures.[1−4] In addition to their fascinating properties,[5−8] these nanocrystals have started to show values in applications ranging from catalysis[9−11] to photonics,[12,13] sensing,[14−18] and biomedical research.[19−22] Despite the promising results reported in many publications, there still exists a major barrier in moving these nanomaterials from academic studies to industrial applications.[23] The barrier can be attributed to the lack of an ability to produce the nanocrystals in large enough quantities while maintaining the uniformity and precise controls over their physicochemical properties. People have sought to increase the volume of production by switching to larger reactors and thus higher volumes of reagents. However, the increase in volume often results in products with nonuniformity and poor controls because both the nucleation and growth of colloidal nanocrystals are extremely sensitive to the experimental details, including heat management, temperature variation, and the way reagents are introduced and mixed. These parameters usually have nonlinear correlations with the volume of reaction solution and thus cannot be easily scaled up in a linear fashion.

An alternative approach to nanocrystal synthesis is based on the use of reactors in the form of a continuous flow of small droplets.[24−26] This new approach offers many attractive features for scalable production, including fast rates for thermal and mass transfer in a relatively small volume,[27] the capability to run many syntheses in parallel and in continuous flow,[28,29] and the low consumption of reagents during the process of optimization.[30] Compared to the one-phase, continuous flow synthesis,[31,32] droplet reactors can eliminate dispersion of solutes along the flow channel, leading to more uniform reaction time and thus better controlled products. In recent years, many protocols originally developed using batch reactors have been modified and then successfully extended to droplet reactors. Nanoparticles with a variety of compositions, including noble metals,[33−37] inorganic semiconductors commonly used for quantum dots,[31,38,39] metal oxides,[40−42] and silica,[43,44] have all been prepared using droplet reactors. For noble-metal nanocrystals, however, the products were often troubled by polydispersity and/or lack of controls over the size, shape, and structure.[33−35] This situation is understandable because the droplet reactors are different from batch reactors in mixing, multiphase mass transfer, and surface-to-volume ratio, among others. One has to understand the fundamental

Received: May 28, 2014
Revised: June 18, 2014

   dx.doi.org/10.1021/nl501994q | *Nano Lett.* XXXX, XXX, XXX−XXX

differences between these two systems before the success of a batch synthesis can be duplicated in the droplet-based platform. For example, recent demonstrations indicate that introducing a mixing zone could greatly improve the uniformity of the Pd nanocubes,[45] and a carrier phase had to be carefully selected for reactions involving gasesous species or oxidative etching in order to control the size, shape, and twin structure of the products.[46]

Because all the droplet reactors are operated at much higher surface-to-volume ratios than a batch reactor, interfacial adsorption of nanocrystals, a well-documented phenomenon,[47−49] might have an immediate impact on the outcome of a synthesis. To our knowledge, the effect of interfacial adsorption of colloidal nanocrystals on their synthesis in droplet reactors has not been discussed in literature, probably because some of the capping agents or colloidal stabilizers involved in the syntheses can effectively passivate the water−oil interface (e.g., cetyltrimethylammonium bromide (CTAB) typically employed in the synthesis of Au nanorods[50]) or generate strongly hydrophilic nanocrystals (e.g., Br^-, commonly used in the synthesis of Pd nanocubes[45]) and thus suppress the interfacial adsorption of nanocrystals. However, it should be emphasized that the capping agents or stabilizers used in many of the protocols could not serve as a surfactant to passivate the water−oil interface and the nanocrystals could take an amphiphilic surface when a polymeric capping agent is used. In these cases, the nanocrystals have a strong tendency to be concentrated at the water−oil interface (even for a batch synthesis) to even generate close-packed arrays over large areas.[51,52] As a matter of fact, the water−oil interface has been explored as a versatile platform to fabricate asymmetric nanoparticles.[53,54] Here we systematically investigate the pros and cons of interfacial adsorption in the synthesis of colloidal nanocrystals based on droplet reactors. While interfacial adsorption can be utilized to generate nanocrystals with asymmetric structures, it has to be mitigated through the introduction of a proper surfactant to obtain nanocrystals with a uniform, well-controlled size and shape.

Figure 1a shows a schematic of the fluidic device we used for generating droplet reactors. The carrier phase (in the present work, silicone oil) and aqueous solutions of the reagents (R1 and R2) were delivered at individually adjustable flow rates using syringe pumps. It is worth noting that we can control the volume of each droplet and the ratio of different reagents in a droplet by varying the flow rates for the carrier phase and reagents, respectively. A mixing zone was introduced to induce chaotic advection and recirculation of reagents in an effort to improve their mixing in each droplet.[45] As a major advantage over the microfabricated, on-chip fluidic device, we could easily cut or extend the polytetrafluoroethylene (PTFE) tube to any desired length to adjust the residence time or reaction time. Typically, the flow rates of silicone oil, R1, and R2 were set to 200, 20, and 20 μL/min, generating droplets of ca. 120 nL in volume in a PTFE tube with an inner diameter of 0.5 mm (see the optical micrograph in Figure 1a). For a 6 m long tube, the reaction time was ca. 5 min. We used the seeded growth of Ag nanocubes and the galvanic replacement between Ag nanocubes and $HAuCl_4$ as two typical examples to examine the impacts of interfacial adsorption on the formation of colloidal metal nanocrystals in droplet reactors.

Figure 1b shows an illustration of the seeded growth involving the use of Ag nanocubes as the seeds in the presence of poly(vinylpyrrolidone) (PVP) as a capping agent. The

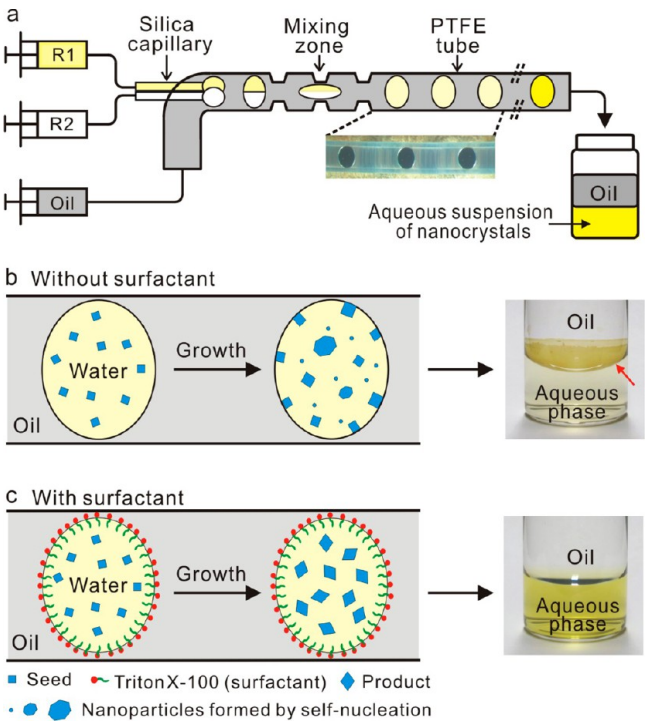

Figure 1. (a) A schematic of the experimental setup used for the generation of aqueous droplets separated by oil, followed by mixing of the reagents and formation of nanocrystals in the droplets. Inset: photograph of droplets containing blue food dye in a PTFE tube. (b,c) Schematics and photographs showing how to control interfacial adsorption of nanocrystals at the water−oil interface with a surfactant. (b) Nanocrystals are prone to adsorption at a surfactant-free water−oil interface during a reaction, leading to self-nucleation in the droplets. The photograph shows the product collected from a seeded growth of Ag nanocubes in droplet reactors with PVP as a capping agent. The majority of the products concentrated at the water−oil meniscus marked by the red arrow. (c) When the seeded growth of Ag nanocubes was conducted in the presence of Triton X-100 (0.55% by wt.), no obvious interfacial adsorption was observed as shown by the strong yellow color from the aqueous phase in the vial.

nanocrystals were well dispersed in each droplet at the very beginning of a growth process due to fast mixing in the droplets. During the synthesis, however, the nanocrystals would gradually adsorb onto the water−oil interface. As a result, the number of seeds remaining in the aqueous phase constantly dropped as the reaction time was prolonged. The ratio of seeds to precursor molecules (or atoms derived from the precursor) gradually decreased with reaction time as well. As the ratio dropped below a critical level, irregular nanoparticles would start to appear via a homogeneous nucleation pathway. When the final products were collected in a glass vial, most of the particles were concentrated at the water−oil interface (i.e., the meniscus marked by an arrow) while the aqueous phase only showed a very light yellow color (see the photograph in Figure 1b).

Similar to a bulk system, the interfacial adsorption phenomenon can be utilized to generate nanocrystals with asymmetric shapes or structures. As shown in Figure 2a, we modified the setup in Figure 1a by eliminating the mixing zone and allowing the Ag nanocubes in reagent R1 to adsorb onto the water−oil interface prior to the introduction of reagent R2 (CF_3COOAg or $HAuCl_4$ depending on seeded growth or galvanic replacement). The flow rates of silicone oil, R1, and R2

dx.doi.org/10.1021/nl501994q | Nano Lett. XXXX, XXX, XXX−XXX

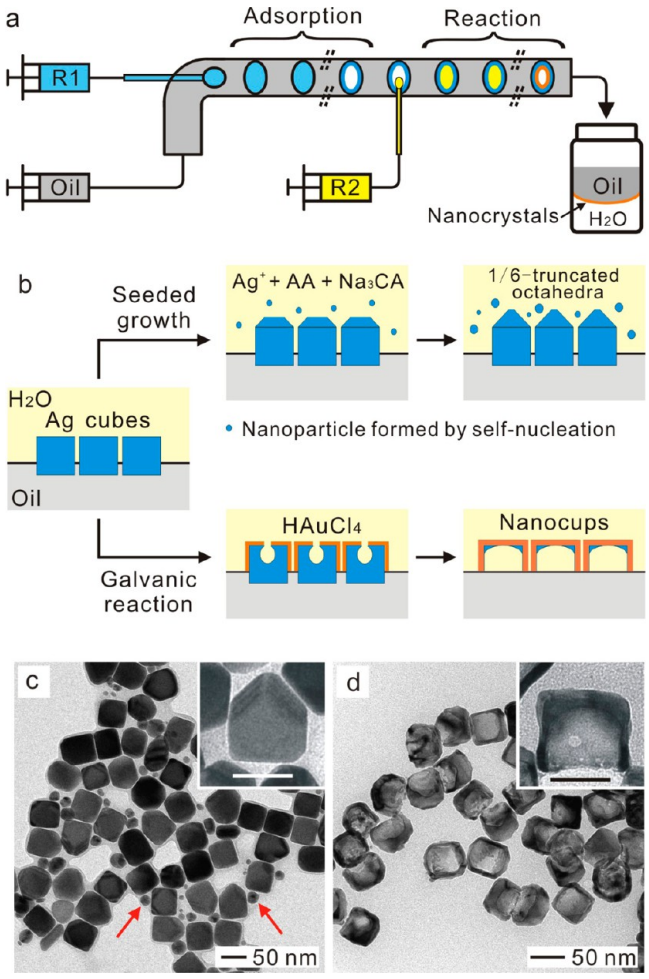

Figure 2. (a) Schematic illustration of the experimental setup used for the synthesis of asymmetric nanocrystals. The seeds or templates in R1 were allowed to adsorb onto the water−oil interface of droplets prior to the injection of R2 to initiate the reaction. (b) Schematic illustration of the seeded growth and galvanic reaction at the water−oil interface. (c,d) TEM images of asymmetric nanocrystals: (c) one-sixth-truncated Ag octahedra together with tiny particles (marked by arrows) formed through self-nucleation, and (d) Au−Ag nanocups. The scale bars in the insets correspond to 40 nm.

were set to 120, 20, and 10 μL/min. The lengths of PTFE segments for adsorption and reaction were both set to 3 m, resulting in a reaction time of ca. 4 min. During collection, Triton X-100 was added to help transfer the products from the water−oil interface into an aqueous phase, followed by sonication and centrifugation. Figure 2b shows schematic illustrations of the asymmetric growth and galvanic replacement reaction involving Ag nanocubes adsorbed at the water−oil interface of a droplet. A packing of nanocrystals close to a monolayer could be formed at the interface by controlling the amount of seeds added into each droplet. For each Ag nanocube at the interface, only the portion exposed to the aqueous phase was able to participate in the seeded growth or galvanic replacement. When R2 contained CF_3COOAg, L-ascorbic acid (AA), and Na_3CA (as precursor, reductant, and capping agent, respectively), the Ag nanocubes evolved into one-sixth-truncated octahedra,[55] together with some tiny particles (marked by arrows) formed through self-nucleation (Figure 2c). It is worth noting that it was hard to suppress self-nucleation because most of the Ag nanocubes were adsorbed at the water−oil interface, leaving behind very few seeds in the aqueous phase. If necessary, the tiny particles formed via self-nucleation could be separated from the product by adjusting the speed of centrifugation. As for the galvanic replacement reaction, the products were Au−Ag nanocups instead of nanocages. In the early stage, a pinhole was formed in the front portion of each Ag nanocube in contact with the aqueous phase, and a void was developed at a later stage, accompanied by the deposition and diffusion of Au atoms to five of the six faces. Because the Au atoms could not reach the portion of the Ag nanocube immersed in the oil phase, the final product would become a cubic nanocup after the Ag nanocube had been completely reacted with the $HAuCl_4$ added into each droplet. Figure 2d shows a typical TEM image of the as-obtained nanocups, characterized by a cubic cavity and a wall thickness of ca. 5 nm.

We also characterized the localized surface plasmon resonance (LSPR) properties of the nanocrystals with asymmetric structures. Supporting Information Figure S1 shows normalized UV−vis spectra recorded from aqueous suspensions of the one-sixth-truncated Ag octahedra (Figure 2c), the Au−Ag nanocups (Figure 2d), and the corresponding normal Ag octahedra (ca. 65 nm in size) and Au−Ag nanocages that were prepared using 40 nm Ag cubes as seeds and templates, respectively. The major LSPR peak of the one-sixth-truncated Ag octahedra showed a blueshift of 11 nm relative to the Ag octahedra, and the peaks located at 350 and 380 nm were increased in intensity. For the Au−Ag nanocups, the major LSPR peak located at 709 nm was broader than that of the Au−Ag nanocages. In addition, two shoulder peaks were observed at 475 and 512 nm. These differences can be attributed to a lower symmetry for the one-sixth-truncated Ag octahedra and nanocups, resulting in more different ways to polarize the electrons.[56]

In many cases, interfacial adsorption of nanocrystals should be avoided in order to preserve the uniformity of nanocrystals serving as seeds or templates and, at the same time, help achieve tight controls over their sizes, shapes, and structures. The simplest approach is to add a surfactant into the droplet, which should effectively passivate the water−oil interface to diminish interfacial adsorption of nanocrystals while presenting no interference with the growth or reaction on the seeds or templates. Inspired by the work on the reduction of nonspecific adsorption of proteins and peptides in a plug-based microfluidic system,[57,58] we found that the interfacial adsorption of nanocrystals in droplet reactors could be effectively mitigated by adding Triton X-100 into the aqueous phase. As a nonionic surfactant, Triton X-100 is particularly interesting because it will not introduce any ionic species (e.g., Br^- and Cl^-) that may react with the precursor (e.g., Ag^+). As shown in Figure 1c, the Triton X-100 molecules tend to be arranged at the water−oil interface with the hydrophilic chain and hydrophobic head in the aqueous and oil phases, respectively. Because the water−oil interface is now passivated by the surfactant, the nanocrystals will remain to be dispersed in the aqueous phase during the entire course of a reaction, resulting in products with a uniform size, shape, and structure. When we conducted the growth of Ag nanocubes in aqueous droplets in the presence of Triton X-100 (0.55% by wt.), no obvious adsorption of nanocrystals was observed at the water−oil interface as shown by the photograph in Figure 1c. The aqueous phase showed a bright yellow color, indicating that the Ag nanocrystals were well dispersed in the aqueous phase. Also, the water−oil interface formed a flat

dx.doi.org/10.1021/nl501994q | Nano Lett. XXXX, XXX, XXX−XXX

meniscus in the presence of Triton X-100. This result confirms that the addition of Triton X-100 could effectively prevent the nanocrystals from adsorption onto the water−oil interface.

To quantify the interfacial adsorption of nanocrystals, we determined the percentage of Ag nanocubes adsorbed onto the water−oil interface by measuring the intensity of LSPR peak associated with the nanocubes remaining in the aqueous phase. The detailed procedures can be found in the Supporting Information. First, we investigated the effect of particle size on the interfacial adsorption of nanocrystals by dispersing 22, 40, and 90 nm Ag cubes (Supporting Information Figure S2) in deionized (DI) water and then by dispersing them into droplets separated by silicone oil. The nanocubes were then collected from the aqueous phase and analyzed using UV−vis spectroscopy. We found that interfacial adsorption was less significant for smaller nanocubes as compared with their larger counterparts, which is consistent with a previous report.[47] In addition, increasing the length of the PTFE tube led to more significant adsorption of the nanocubes to the water−oil interface (Supporting Information Figure S3a). When only PVP or Na_3CA was added into the droplets at a certain concentration, we found that more than 70% of the 22 nm Ag cubes adsorbed to the water−oil interface after the droplets had flowing through a 2 m long PTFE tube (Supporting Information Figure S3b). When we extended the length of the PTFE tube to 6 m, ca. 90% of the 22 nm Ag cubes were concentrated at the water−oil interface in the presence of Na_3CA. As expected, the addition of Triton X-100 could completely prevent the Ag nanocubes from adsorption to the water−oil interface (Supporting Information Figure S3b).

Other than mitigating the interfacial adsorption of nanocrystals, the Triton X-100 was found to have no impact on the seeded growth or galvanic reaction of the nanocrystals. For example, when the galvanic replacement reaction between 40 nm Ag cubes and $HAuCl_4$ was conducted in the droplets containing Triton X-100, we obtained products with both uniform size and shape. As shown in Figure 3a−d, the 40 nm Ag cubes evolved into Au−Ag nanocages as the concentration of $HAuCl_4$ in the reagent R2 was increased. The major LSPR peaks of these nanostructures showed a constant redshift from 479 to 570, 748, and 830 nm (Supporting Information Figure S4a). For comparison, TEM images of the products obtained in the absence of Triton X-100 were also presented (Figure 3e−h). Although a similar evolution in morphology was observed, the samples were troubled by polydispersity. For example, when the concentration of $HAuCl_4$ in the reagent R2 was 0.18 mM, small Au nanoparticles were also found in the products (Figure 3h) due to the involvement of significant dealloying. This result implies that the galvanic replacement reaction did not proceed at the same pace for the different Ag nanocubes owing to their continuous adsorption to the water−oil interface. As shown in Supporting Information Figure S4b, the major LSPR peaks recorded from the products obtained in the absence of Triton X-100 were broader than those shown in Supporting Information Figure S4a. According to the TEM images in Figure 3e−h, the peak broadening can be attributed to a broader range of void sizes and shapes for the resultant hollow nanostructures.

We further evaluated the effect of Triton X-100 on the capping agent by performing seeded growth of Ag nanocrystals in the droplets. When a certain amount of CF_3COOAg (precursor) was introduced into the aqueous droplets containing AA (reductant), 22 nm Ag cubes (seeds, see

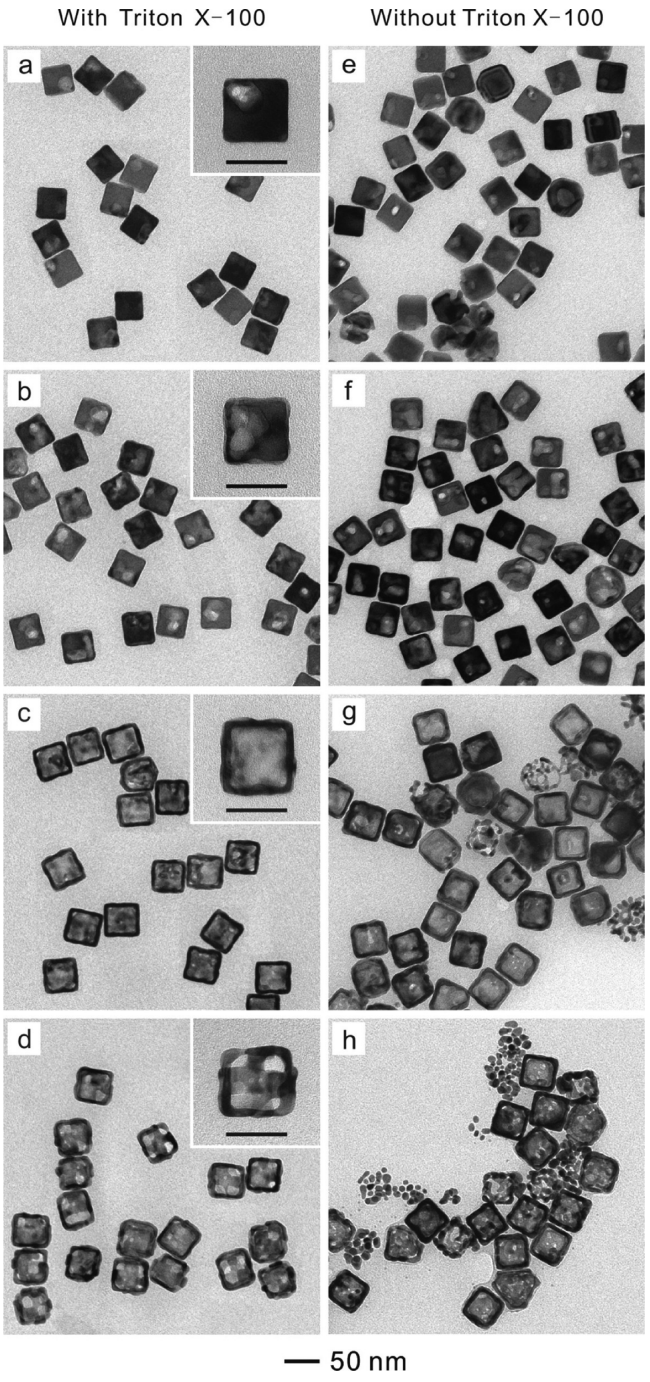

Figure 3. TEM images showing the structural evolution of 40 nm Ag cubes into Au−Ag nanoboxes and nanocages in the presence (left column) and absence (right column) of Triton X-100. The concentration of $HAuCl_4$ in the reagent R2 was (a,e) 0.02 mM, (b,f) 0.04 mM, (c,g) 0.10 mM, and (d,h) 0.18 mM, respectively. The scale bars in the insets correspond to 40 nm.

Supporting Information Figure S2a), PVP (capping agent), and Triton X-100 at room temperature, we obtained uniform Ag nanocubes of 25 nm in edge length (Figure 4a). As expected, the same batch of Ag seeds grew into octahedra covered by {111} facets when the PVP was substituted by Na_3CA (Figure 4c). These results are consistent with our previous observations for batch-based syntheses.[59] In comparison, Figure 4b,d shows TEM images obtained from control experiments conducted in the absence of Triton X-100. In these cases, Ag nanocrystals

dx.doi.org/10.1021/nl501994q | *Nano Lett.* XXXX, XXX, XXX−XXX

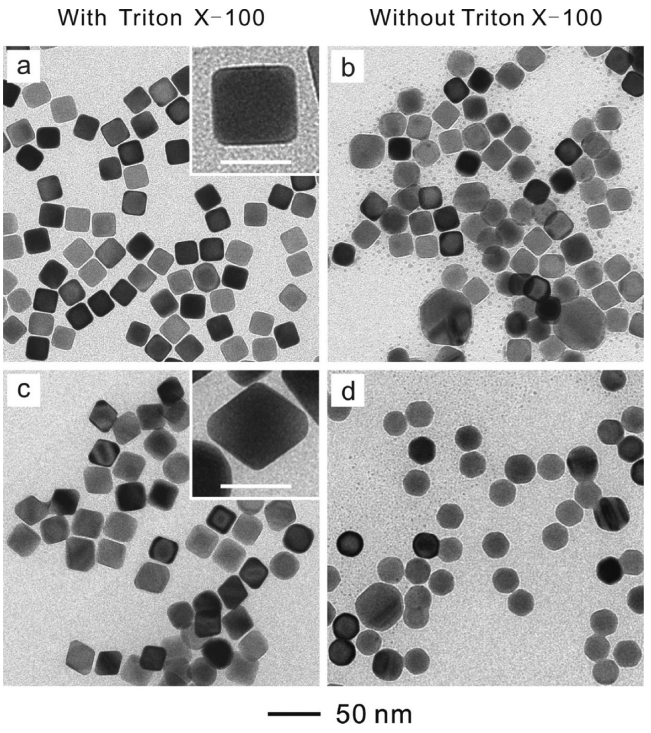

Figure 4. (a,b) TEM images of Ag nanocubes that were prepared using seeded growth with PVP as a capping agent in the presence and absence of Triton X-100, respectively. (c,d) TEM images of Ag octahedra that were prepared using seeded growth with Na_3CA as a capping agent in the presence and absence of Triton X-100, respectively. The scale bars in the insets correspond to 20 nm. In the absence of Triton X-100, the concentration of seeds in the droplets decreased with reaction time due to interfacial adsorption, resulting in self-nucleation and formation of small particles, in addition to some large particles with irregular shapes.

with irregular shapes were found in the final products due to self-nucleation since most of the seeds adsorbed onto the water−oil interface, leaving behind fewer seeds in the aqueous phase for growth. As shown in Figure 4d, most of the cubic Ag seeds evolved into cuboctahedra smaller than the octahedra shown in Figure 4c due to the consumption of the precursor through self-nucleation. Taken together, we can conclude that Triton X-100 does not affect the capping effect of PVP and Na_3CA and is able to effectively passivate the droplet−carrier interface and suppress the interfacial adsorption of seeds, leading to the formation of uniform nanocrystals in the droplets.

In summary, we have systematically investigated the effects of interfacial adsorption on the synthesis of colloidal nanocrystals in droplet reactors. First, we demonstrated the use of a droplet system for the synthesis of asymmetric nanocrystals by concentrating the seeds or templates at the water−oil interface prior to reaction. As a result, one-sixth-truncated Ag octahedra and Au−Ag nanocups were obtained when Ag nanocubes were used as the seeds for growth and as the templates for a galvanic replacement reaction with $HAuCl_4$, respectively. On the other hand, interfacial adsorption of nanocrystals could be avoided by adding a surfactant in advance to passivate the water−oil interface and thus obtain uniform products with a well-controlled size and shape. We demonstrated that Triton X-100, a nonionic surfactant, could effectively suppress the interfacial adsorption of nanocrystals and help maintain their uniformity in terms of both size and shape. Significantly, Triton X-100 does not affect the capping effect of PVP and Na_3CA for Ag(100) and Ag(111) surfaces, respectively. By understanding the pros and cons of interfacial adsorption in droplet reactors, we will be able to develop a general platform for the scalable production of colloidal nanocrystals with controlled sizes, shapes, compositions, and structures.

■ ASSOCIATED CONTENT

Supporting Information

The methods and experimental procedures are provided, together with four additional figures (Figures S1−S4): UV−vis spectra recorded from aqueous suspensions of the one-sixth-truncated Ag octahedra, the nanocups, and the corresponding normal Ag octahedra (ca. 65 nm in size) and Au−Ag nanocages that were prepared using 40 nm Ag cubes as seeds and templates, respectively; TEM images of the Ag nanocubes with different edge lengths; percentages of Ag nanocubes adsorbed at the water−oil interface of droplets as a function of the length of the PTFE tube; and UV−vis spectra taken from aqueous suspensions of samples shown in Figure 3. This material is available free of charge via the Internet at http://pubs.acs.org.

■ AUTHOR INFORMATION

Corresponding Author

*E-mail: younan.xia@bme.gatech.edu.

Notes

The authors declare no competing financial interest.

■ ACKNOWLEDGMENTS

This work was supported by startup funds from the Georgia Institute of Technology. As a visiting scholar from Zhejiang University, L.Z. was also partially supported by the National Natural Science Foundation of China (Project Nos. 61036012 and 61275217). As a visiting Ph.D. student from Southwest University, Y.W. was also partially supported by a fellowship from the China Scholarship Council.

■ REFERENCES

(1) Tao, A. R.; Habas, S.; Yang, P. *Small* **2008**, *4*, 310−325.
(2) Xia, Y.; Xiong, Y.; Lim, B.; Skrabalak, S. E. *Angew. Chem., Int. Ed.* **2009**, *48*, 60−103.
(3) Sau, T. K.; Rogach, A. L. *Adv. Mater.* **2010**, *22*, 1781−1804.
(4) Xia, Y.; Xia, X.; Wang, Y.; Xie, S. *MRS Bull.* **2013**, *38*, 335−344.
(5) Narayanan, R.; El-Sayed, M. A. *Nano Lett.* **2004**, *4*, 1343−1348.
(6) Tian, N.; Zhou, Z.; Sun, S.; Ding, Y.; Wang, Z. *Science* **2007**, *316*, 732−735.
(7) Zhang, J.; Langille, M. R.; Personick, M. L.; Zhang, K.; Li, S.; Mirkin, C. A. *J. Am. Chem. Soc.* **2010**, *132*, 14012−14014.
(8) Chen, H.; Shao, L.; Li, Q.; Wang, J. *Chem. Soc. Rev.* **2013**, *42*, 2679−2724.
(9) Zhang, H.; Jin, M.; Xia, Y. *Angew. Chem., Int. Ed.* **2012**, *51*, 7656−7673.
(10) Huang, X.; Li, Y.; Li, Y.; Zhou, H.; Duan, X.; Huang, Y. *Nano Lett.* **2012**, *12*, 4265−4270.
(11) Wu, J.; Yang, H. *Acc. Chem. Res.* **2013**, *46*, 1848−1857.
(12) Pyayt, A. L.; Wiley, B.; Xia, Y.; Chen, A.; Dalton, L. *Nat. Nanotechnol.* **2008**, *3*, 660−665.
(13) Xiong, X.; Zou, C.; Ren, X.; Liu, A.; Ye, Y.; Sun, F.; Guo, G. *Laser Photonics Rev.* **2013**, *7*, 901−919.
(14) Anker, J. N.; Hall, W. P.; Lyandres, O.; Shah, N. C.; Zhao, J.; Van Duyne, R. P. *Nat. Mater.* **2008**, *7*, 442−453.
(15) Gao, C.; Lu, Z.; Liu, Y.; Zhang, Q.; Chi, M.; Cheng, Q.; Yin, Y. *Angew. Chem., Int. Ed.* **2012**, *51*, 5629−5633.

(16) Grzelczak, M.; Liz-Marzán, L. M. *Langmuir* **2013**, *29*, 4652−4663.
(17) Chiu, C.-Y.; Huang, M. H. *Angew. Chem., Int. Ed.* **2013**, *52*, 12709−12713.
(18) Abbas, A.; Tian, L.; Morrissey, J. J.; Kharasch, E. D.; Singamaneni, S. *Adv. Funct. Mater.* **2013**, *23*, 1789−1797.
(19) Loo, C.; Lowery, A.; Halas, N.; West, J.; Drezek, R. *Nano Lett.* **2005**, *5*, 709−711.
(20) Xia, Y.; Li, W.; Cobley, C. M.; Chen, J.; Xia, X.; Zhang, Q.; Yang, M.; Cho, E. C.; Brown, P. K. *Acc. Chem. Res.* **2011**, *44*, 914−924.
(21) Dreaden, E.; Huang, X.; Alkilany, A. M.; Murphy, C. J.; El-Sayed, M. A. *Chem. Soc. Rev.* **2012**, *41*, 2740−2779.
(22) Lohse, S. E.; Murphy, C. J. *J. Am. Chem. Soc.* **2012**, *134*, 15607−15620.
(23) Zhang, L.; Xia, Y. *Adv. Mater.* **2014**, *26*, 2600−2606.
(24) Song, H.; Tice, J. D.; Ismagilov, R. F. *Angew. Chem., Int. Ed.* **2003**, *42*, 768−772.
(25) Song, Y. J.; Hormes, J.; Kumar, C. S. S. R. *Small* **2008**, *4*, 698−711.
(26) Nightingale, A. M.; deMello, J. C. *Adv. Mater.* **2013**, *25*, 1813−1821.
(27) Song, H.; Chen, D.; Ismagilov, R. F. *Angew. Chem., Int. Ed.* **2006**, *45*, 7336−7356.
(28) Bannock, J. H.; Krishnadasan, S. H.; Nightingale, A. M.; Yau, C. P.; Khaw, K.; Burkitt, D.; Halls, J. J. M.; Heeney, M.; de Mello, J. C. *Adv. Funct. Mater.* **2013**, *23*, 2123−2129.
(29) Nightingale, A. M.; Bannock, J. H.; Krishnadasan, S. H.; O'Mahony, F. T. F.; Haque, S. A.; Sloan, J.; Drury, C.; McIntyre, R.; deMello, J. C. *J. Mater. Chem. A* **2013**, *1*, 4067−4076.
(30) Theberge, A. B.; Courtois, F.; Schaerli, Y.; Fischlechner, M.; Abell, C.; Hollfelder, F.; Huck, W. T. S. *Angew. Chem., Int. Ed.* **2010**, *49*, 5846−5868.
(31) Kwon, B.-H.; Lee, K. G.; Park, T. J.; Kim, H.; Lee, T. J.; Lee, S. J.; Jeon, D. Y. *Small* **2012**, *8*, 3257−3262.
(32) Lohse, S. E.; Eller, J. R.; Sivapalan, S. T.; Plews, M. R.; Murphy, C. J. *ACS Nano* **2013**, *7*, 4135−4150.
(33) Duraiswamy, S.; Khan, S. A. *Small* **2009**, *5*, 2828−2834.
(34) Cabeza, V. S.; Kuhn, S.; Kulkarni, A. A.; Jensen, K. F. *Langmuir* **2012**, *28*, 7007−7013.
(35) Knauer, A.; Csáki, A.; Möller, F.; Hühn, C.; Fritzsche, W.; Köhler, J. M. *J. Phys. Chem. C* **2012**, *116*, 9251−9258.
(36) LLazarus, L. L.; Riche, C. T.; Marin, B. C.; Gupta, M.; Malmstadt, N.; Brutchey, R. L. *ACS Appl. Mater. Interfaces* **2012**, *4*, 3077−3083.
(37) Khan, S. A.; Duraiswamy, S. *Lab Chip* **2012**, *12*, 1807−1812.
(38) Shestopalov, I.; Tice, J. D.; Ismagilov, R. F. *Lab Chip* **2004**, *4*, 316−321.
(39) Chan, E. M.; Alivisatos, A. P.; Mathies, R. A. *J. Am. Chem. Soc.* **2005**, *127*, 13854−13861.
(40) Frenz, L.; El Harrak, A.; Pauly, M.; Begin-Colin, S.; Griffiths, A. D.; Baret, J. C. *Angew. Chem., Int. Ed.* **2008**, *47*, 6817−6820.
(41) Hoang, P. H.; Park, H.; Kim, D. P. *J. Am. Chem. Soc.* **2011**, *133*, 14765−14770.
(42) Nightingale, A. M.; Krishnadasan, S. H.; Berhanu, D.; Niu, X.; Drury, C.; McIntyre, R.; Valsami-Jones, E.; deMello, J. C. *Lab Chip* **2011**, *11*, 1221−1227.
(43) Lee, S.-K.; Liu, X.; Sebastian Cabeza, V.; Jensen, K. F. *Lab Chip* **2012**, *12*, 4080−4084.
(44) Wacker, J. B.; Lignos, I.; Parashar, V. K.; Gijs, M. A. M. *Lab Chip* **2012**, *12*, 3111−3116.
(45) Kim, Y. H.; Zhang, L.; Yu, T.; Jin, M.; Qin, D.; Xia, Y. *Small* **2013**, *9*, 3462−3467.
(46) Zhang, L.; Wang, Y.; Tong, L.; Xia, Y. *Langmuir* **2013**, *29*, 15719−15725.
(47) Lin, Y.; Skaff, H.; Emrick, T.; Dinsmore, A. D.; Russell, T. P. *Science* **2003**, *299*, 226−229.
(48) Binder, W. H. *Angew. Chem., Int. Ed.* **2005**, *44*, 5172−5175.
(49) Cecchini, M. P.; Turek, V. A.; Paget, J.; Kornyshev, A. A.; Edel, J. B. *Nat. Mater.* **2013**, *12*, 165−171.
(50) Nikoobakht, B.; El-Sayed, M. A. *Chem. Mater.* **2003**, *15*, 1957−1962.
(51) Cheng, L.; Liu, A.; Peng, S.; Duan, H. *ACS Nano* **2010**, *4*, 6098−6104.
(52) Turek, V. A.; Cecchini, M. P.; Paget, J.; Kucernak, A. R.; Kornyshev, A. A.; Edel, J. B. *ACS Nano* **2012**, *6*, 7789−7799.
(53) Niu, Z.; He, J.; Russell, T. P.; Wang, Q. *Angew. Chem., Int. Ed.* **2010**, *49*, 10052−10066.
(54) He, J.; Perez, M. T.; Zhang, P.; Liu, Y.; Babu, T.; Gong, J.; Nie, Z. *J. Am. Chem. Soc.* **2012**, *134*, 3639−3642.
(55) Xia, X.; Xia, Y. *Nano Lett.* **2012**, *12*, 6038−6042.
(56) Wiley, B. J.; Im, S. H.; Li, Z.; McLellan, J.; Siekkinen, A.; Xia, Y. *J. Phys. Chem. B* **2006**, *110*, 15666−15675.
(57) Roach, L. S.; Song, H.; Ismagilov, R. F. *Anal. Chem.* **2005**, *77*, 785−796.
(58) Meier, M.; Kennedy-Darling, J.; Choi, S. H.; Norstrom, E. M.; Sisodia, S. S.; Ismagilov, R. F. *Angew. Chem., Int. Ed.* **2009**, *48*, 1487−1489.
(59) Zeng, J.; Zheng, Y.; Rycenga, M.; Tao, J.; Li, Z.; Zhang, Q.; Zhu, Y.; Xia, Y. *J. Am. Chem. Soc.* **2010**, *132*, 8552−8553.